Measurement of the QED energy shift in the $1s^2 2p_{3/2} - 1s^2 2s_{1/2}$ x-ray transition in Li-like $^{208}Pb^{79+}$

Xuemei Zhang,[1,*] Nobuyuki Nakamura,[2] Chongyang Chen,[1] Martin Andersson,[1] Yong Liu,[1] and Shunsuke Ohtani[2]
[1]*EBIT Laboratory, Institute of Modern Physics, Fudan University, Shanghai 200433, People's Republic of China and the Key Laboratory of Applied Ion Beam Physics, Ministry of Education, People's Republic of China*
[2]*Institute of Laser Science, The University of Electro-Communications, Chofu 182-8585, Japan*
(Received 11 April 2008; revised manuscript received 13 July 2008; published 4 September 2008)

The $1s^2 2p_{3/2} - 1s^2 2s_{1/2}$ x-ray transition in the Li-like Pb^{79+} has been observed using the Tokyo electron beam ion trap at the University of Electro-Communications. The contribution of QED (-24.99 ± 0.10 eV) to the $1s^2 2p_{3/2} - 1s^2 2s_{1/2}$ transition in $^{208}Pb^{79+}$ is determined and compared with different calculations. The measurement was made by calibrating the Pb line using the Lyman-α lines of the H-like *S* and the $1s4p\ ^1P_1 - 1s^2\ ^1S_0$ transition in the He-like *P*.

DOI: 10.1103/PhysRevA.78.032504 PACS number(s): 31.30.J−, 12.20.Fv, 32.30.Rj

I. INTRODUCTION

With the developing of modern ion source and accelerator technologies, more and more kinds of ions can be produced, including few-electron ions for the heaviest elements. Interest in the precise atomic structure of few-electron ions in heavy elements increased considerably in the last decade. Precise determination of the accurate structure of highly charged ions is very helpful for a detailed understanding of quantum-electrodynamics (QED) in strong fields.

As mentioned in many papers [1–6], measurements of the Li-like systems can provide data to be more sensitive to higher-order QED terms than those of H-like systems, though the calculation of QED terms for the Li-like ions is more complex than that for the H-like ions due to the presence of two additional electrons. The treatment of QED in the many-particle environment is still a field in development.

In this paper, the x-ray transition in the Li-like Pb^{79+}, $1s^2 2p_{3/2} - 1s^2 2s_{1/2}$, was investigated by using the flat crystal spectrometer at the Tokyo electron beam ion trap (EBIT) [7].

II. EXPERIMENT

The experimental setup used in the present study is shown in Fig. 1. The Tokyo EBIT was used to produce and trap the Li-like Pb^{79+}. The electron energy was 90 keV and the current was 200–230 mA. Pb was injected into the EBIT using an effusion cell [8]. The x-ray transition in the Li-like Pb^{79+}, $1s^2 2p_{3/2} - 1s^2 2s_{1/2}$, was observed with a flat crystal x-ray spectrometer that consisted of a Si(111) crystal and a back-illuminated CCD. Although a position sensitive proportional counter [9] used to be a detector, in this study a back illuminated charge-coupled device (CCD) was used because it could be used in vacuum without any window, so that it had high quantum efficiency for the objective x-ray energy range ($\sim$2.5 keV).

The charge state distribution was investigated through x-ray observation with a Ge detector. Figure 2 shows the radiative recombination (RR) x-ray spectra obtained with different experimental conditions. The main difference was the trap potential (the potential-well depth at the ion trap). Trap potential was 40 V to obtain the upper spectrum, and 100 V for the lower one. It can be seen from Fig. 2 that the recombination peak into the $n=2$ shell is split into two components: One into $j=3/2$ levels and the other into $j=1/2$ levels. The relative ratio of the $j=1/2$ to $j=3/2$ feature presents a measure of the charge balance [2]. All charge states higher than Ne-like have a vacancy in the $2p_{3/2}$ subshell and thus can contribute to the $j=3/2$ recombination peak. However, only charge states higher than C-like with a $2s_{1/2}$ or $2p_{1/2}$ vacancy, thus are able to contribute to the $j=1/2$ recombination peak. Therefore, higher peak for $j=1/2$ means more higher charged ions produced in the trap. From the intensity ratio between RR x rays into $n=2$ ($j=1/2$) and $n=2$ ($j=3/2$), it can be seen that the charge state distribution for the upper condition is higher than that for the lower condition. It is confirmed that the charge state distribution could be changed by carefully adjusting the trap potential.

For the wavelength calibration, the Lyman-α transitions in the H-like *S* and the $4p-1s$ transition in the He-like *P* were also observed. Sulfur was injected through a gas injector as SF_6 while phosphorus was injected from the gas injection port using the vapor of diethyl phosphite (liquid).

In order to check for electronic drifts as well as the stability of the source, six spectra of the H-like *S* were recorded in an alternating fashion with six Pb spectra. At last, 10 hours measurement for calibration lines was carried out with injection of *S* and *P* simultaneously.

III. RESULTS

Figure 3 shows the x-ray spectra obtained by the flat crystal spectrometer. The upper figure is obtained under "higher"

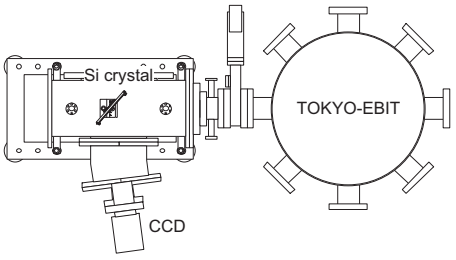

FIG. 1. Experimental setup for x-ray spectroscopy of the Li-like Pb with the Tokyo EBIT.

*zhangxm@fudan.edu.cn

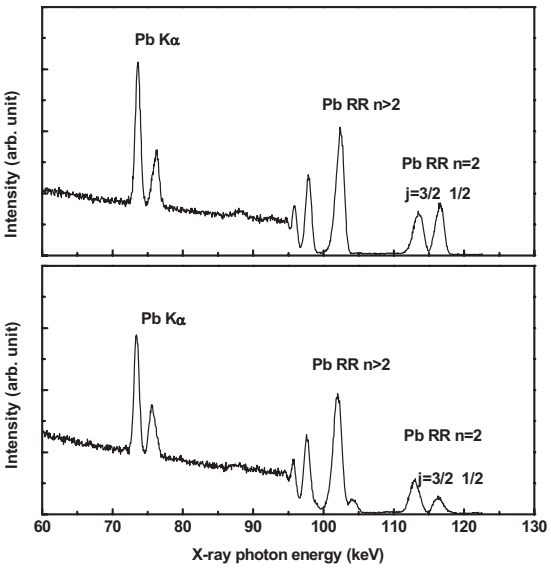

FIG. 2. Radiative recombination x-ray spectra obtained by a Ge detector. Spectra obtained with two different experimental conditions are shown. From the intensity ratio between RR x rays into $n=2$ $(j=3/2)$ and $n=2$ $(j=1/2)$, it can be confirmed that the charge state distribution for the upper condition is higher than that for the lower condition

charge state distribution (upper part in Fig. 2). The middle one corresponds to the "lower" charge state distribution (lower part in Fig. 2). As seen in the figure, it is found that the line at around 2642 eV can be observed only under the "higher" charge state distribution condition. Thus, that line is considered to be the line from the Li-like Pb ions whereas the line at around 2660 eV is considered to be a line from lower charged ions. Based on the discussion in Sec. IV, the lower charge state can be determined to be the N-like. The spectrum of calibration lines for 10 hours measurement is shown in the lower part of Fig. 3. In Fig. 3, the horizontal axis has been calibrated using the Lyman-α lines of the H-like S and the $4p-1s$ transition of the He-like P. The wavelength scale and dispersion of the spectrometer was determined by a quadratic fitting of reference lines.

The method shown in Ref. [10] is used in current experimental data analysis. It is different from the method in Ref. [11], in which the dispersion was determined from the Bragg angle, the crystal-detector distance and the detector angle. Here, wavelength intervals are used to determine experimentally the dispersion of the instrument. The wavelength corresponding to channel x at the detector is expressed as

$$\lambda = \lambda_0 + a(x - x_0) + b(x - x_0)^2 + \cdots , \qquad (1)$$

where λ_0 is the value of wavelength at channel x_0. According to Ref. [10], no more than a few ppm uncertainty is introduced into the determination of wavelengths by the retention of only the linear and quadratic terms. Thus, it can be negligible in current measurement. The dispersion of the spectrometer is determined using the two known intervals between the three reference lines by a quadratic fitting. In the following discussion, it is found that the error arising from

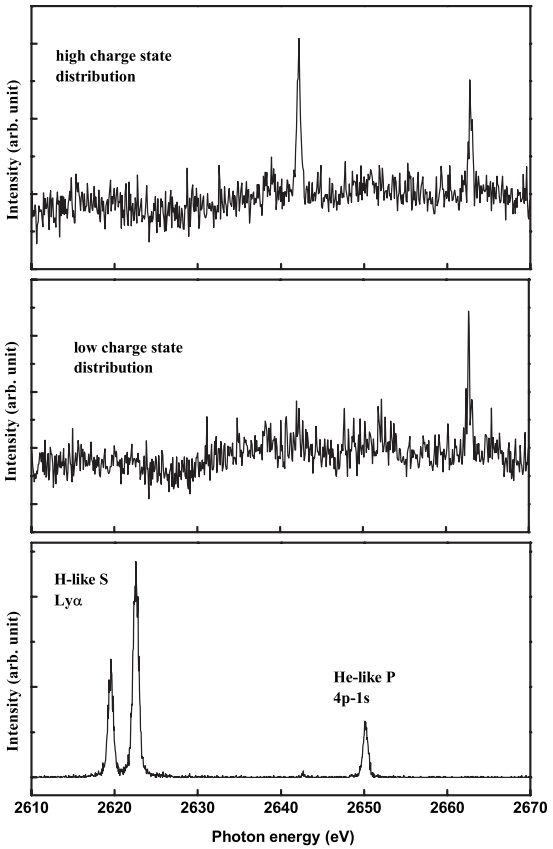

FIG. 3. High resolution x-ray spectra obtained by a flat crystal spectrometer. (Upper) Spectrum of Pb ions obtained under the higher charge state distribution condition. (Middle) Spectrum of Pb ions obtained under the lower charge state distribution condition. (Lower) Spectrum of S and P ions used for the wavelength calibration.

the determination of dispersion function cannot be ignored in the error budget.

As a result, the wavelength of the $1s^2 2p_{3/2} - 1s^2 2s_{1/2}$ transition in $^{208}Pb^{79+}$ has been determined to be 2642.26 ± 0.10 eV and -24.99 ± 0.10 eV obtained for QED contribution. In order to obtain QED contribution, the total non-QED energy 2667.25 eV is subtracted, which includes electronic-structure contribution 2667.31 eV [12], the relativistic recoil correction -0.064 eV [13,14], and the nuclear polarization correction 0.005 eV [15,16].

IV. EXPERIMENTAL UNCERTAINTIES

Satellites, coming from mixing charge state populations, could have significant effect on the results. Although the running parameters of EBIT were optimized to produce the interested Li-like ions, lower charged ions existed inevitably. As discussed in Ref. [2], in EBIT, the electron-impact excitation takes place in the low-collisional limit, and at the same time dielectronic recombination involving only L-shell electrons is energetically forbidden. Therefore, the $2p_{3/2} - 2s_{1/2}$ emission can be understood rather simply, all excitations proceed from the ground state and are followed by radiative decay until they are again back in the ground state. In the

TABLE I. Calculated wavelength and energies of the $2p_{3/2}-2s_{1/2}$ transitions in Pb^{74+} through Pb^{79+}.

Key	Ion	Transition	E_{theory} (Å)	E_{theory} (eV)
Li	Pb^{79+}	$(2p_{3/2})_{J=3/2}-(2s_{1/2})_{J=1/2}$	4.6926	2642.12
Be	Pb^{78+}	$(2s_{1/2}2p_{3/2})_{J=1}-(2s_2)_{J=0}$	4.6132	2687.60
Be-1	Pb^{78+}	$(2s_{1/2}2p_{3/2})_{J=1}-(2s_{1/2}2p_{1/2})_{J=0}$	4.5992	2695.76
Be-2	Pb^{78+}	$(2s_{1/2}2p_{3/2})_{J=1}-(2s_{1/2}2p_{1/2})_{J=1}$	4.6632	2658.71
B-1	Pb^{77+}	$(2s_{1/2}2p_{1/2}2p_{3/2})_{J=3/2}-(2s^22p_{1/2})_{J=1/2}$	4.5731	2711.16
B-2	Pb^{77+}	$(2s_{1/2}2p_{1/2}2p_{3/2})_{J=1/2}-(2s^22p_{1/2})_{J=1/2}$	4.5757	2709.62
B-3	Pb^{77+}	$(2s_{1/2}2p_{1/2}2p_{3/2})_{J=3/2}-(2s^22p_{1/2})_{J=1/2}$	4.7983	2583.94
C	Pb^{76+}	$(2s_{1/2}2p_{1/2}^2 2p_{3/2})_{J=1}-(2s^22p^2)_{J=0}$	4.5203	2742.83
N-1	Pb^{75+}	$(2s_{1/2}2p_{1/2}^2 2p_{3/2}^2)_{J=5/2}-(2s^22p^22p_{3/2})_{J=3/2}$	4.6601	2660.55
N-2	Pb^{75+}	$(2s_{1/2}2p_{1/2}^2 2p_{3/2}^2)_{J=1/2}-(2s^22p^22p_{3/2})_{J=3/2}$	4.4538	2783.78
N-3	Pb^{75+}	$(2s_{1/2}2p_{1/2}^2 2p_{3/2}^2)_{J=3/2}-(2s^22p^22p_{3/2})_{J=3/2}$	4.4520	2784.91
O-1	Pb^{74+}	$(2s_{1/2}2p_{1/2}^2 2p_{3/2}^2)_{J=2}-(2s^22p^22p_{3/2}^2)_{J=2}$	4.5253	2739.80
O-3	Pb^{74+}	$(2s_{1/2}2p_{1/2}^2 2p_{3/2}^2)_{J=1}-(2s^22p^22p_{3/2}^2)_{J=2}$	4.3692	2837.69

following, adjacent transitions from $\Delta n=0$ excitation of a $2s_{1/2}$ electron from nearby highly charged states, from the Li-like to the O-like Pb ions, are calculated and shown in Table I. The GRASPVU package [17–19] based on the multiconfiguration Dirac-Fock (MCDF) method, is employed to calculate the atomic properties. The valence correlation and core-valence correlation [20] from $1s$ and $2s$ subshell electrons are included, and the active space [21,22] is increased systematically to investigate the convergence of the atomic properties. Finally, we allow electrons to be excited up to 4l subshells to generate the configuration state functions (CSF). As for the vacuum polarization (VP), the results from the Fullerton and Rinker work are used [23]. To estimate the contribution of the self-energy (SE), scaling results from one-electron SE shifts are employed [19].

It can be seen that there are two lines close to the $1s^22p_{3/2}-1s^22s_{1/2}$ transition in the Li-like Pb^{79+}, one from the N-like ions (*N*-1 in Table I) and the other from the Be-like ions (Be-2 in Table I). The Be-2 line is produced by excitation of the second possible ground state $(1s^22s_{1/2}2p_{3/2})_{J=0}$ in the Be-like ions. In the absence of a nuclear moment, as in ^{208}Pb, this second possible ground state can only decay via magnetic-dipole, eletric-dipole two-photon decay. Thus, there is a fraction of the Be-like ions occupying this level. According to the calculation in Ref. [2], the intensity of the Be-2 line should be a few percent of the strongest line. If this line appears on the spectrum, it should be rather weak. Therefore, the line at around 2660 eV in Fig. 3 is considered to be the N-1 line from the N-like ions. From Table I, there is no evidence of blending with other lines for the $1s^22p_{3/2}-1s^22s_{1/2}$ transition in the Li-like Pb measurement. However, up to now, transitions with spectator at $n=3$ are not considered. Also in Ref. [2], based on model calculation, the transitions with spectators in the $n=3$ shell are prominent only in the case of the Ne-like ions. Although excitation of a $2s_{1/2}$ electron to the $n=3$ shell can also result in a $2p_{3/2}-2s_{1/2}$ transition in the case of the N-like, the O-like, and the F-like ions, such transitions are never stronger than 3% of the strongest line. For the Ne-like ions, the energies of the transitions are much different from that of the Li-like ions. If transitions with spectators in the $n=3$ shell for the N-like, the O-like, and the F-like ions are included, any satellites with spectator in the $n=3$ shell will be less than a few percent of the intensity of the Li-like line, because from Fig. 3 it can be seen that the intensity of the N-like line is smaller than that of the Li-like line. Thus, any unresolved satellite, even located at a half-width from the centroid of the Li-like line, will cause a shift of no more than 0.01 eV.

During the measurement, in order to check for electronic drifts as well as the stability of the source and the spectrometer, the spectra of the H-like *S* were recorded in an alternating fashion with the Pb spectra. The sums of six Pb spectra and the sums of four *S* spectra are used in the comparison of peak positions. Single Gaussian fitting or single Lorentzian fitting is used in the fitting of the H-like *S* lines and the Pb line. It is determined that the peak position could be reliably found to about ± 0.22 channels, corresponding to about ± 0.022 eV in the present experimental setup. It can also be seen from the above description that the effect of changes in the source position or spectrometer is already included in the ± 0.022 eV uncertainty, since sums of four or six spectra from different measurements are used to determine the peak positions.

Because the He-like *P* line was not observed with the H-like *S* lines in each individual spectrum simultaneously, the uncertainty of the location of the He-like *P* line must be considered. Using the similar analysis as for Pb, similar uncertainty (± 0.22 channels) is obtained for the determination of the He-like *P* peak position. The uncertainty of the locations of the *S* and *P* lines will introduce additional error in the determination of dispersion function. As in Ref. [10], the same quantities are used,

$$q_i = x_{bi} - x_{ai}, \tag{2}$$

$$r_i = x_{ai}^2 - x_{bi}^2 - 2x_0(x_{ai} - x_{bi}) = (x_{ai} + x_{bi})q_i - 2x_0 q_i, \tag{3}$$

where the positions of the two lines which are separated by $\Delta\lambda_i$ are x_{ai} and x_{bi}, x_0 is the position of the calibration line. It follows that $\Delta\lambda_1 = q_1 a + r_1 b$ and $\Delta\lambda_2 = q_2 a + r_2 b$, where a and

b are, respectively, the coefficients of the linear and quadratic terms in Eq. (1). Using the Lyman-α_1 and the He-like *P* line as calibration line, respectively, ± 0.17 eV and ± 0.08 eV are found in the determination of the wavelength for the Pb line due to the uncertainty of the locations of the *S* and *P* lines according to the dispersion relation. That is, the measured line should be closer to the calibration line in order to get higher accuracy. Therefore, in the analysis of current work, the He-like line is used as calibration line. The uncertainty (± 0.08 eV) introduced by the determination of dispersion relation must be included and it is the dominant contribution to the total uncertainty. The much larger uncertainty of the He-like *P* line's wavelength (± 0.044 eV, which is determined in the following paragraph) than that of *S* Lyman-α lines would give larger contribution in the total uncertainty in the determination of the wavelength using Eq. (1). (From Table III, it can be seen that it is the second important contribution to the total uncertainty.)

In the discussion in the last paragraph, $\Delta\lambda_1$ and $\Delta\lambda_2$ are determined by the Lyman-α transitions in the H-like *S* and the $1s4p\ ^1P_1-1s^2\ ^1s_0$ transition in the He-like *P*. The energies of the Lyman-α_1 and Lyman-α_2 lines in S^{15+} are well known as 2622.70 and 2619.70 eV [24]. The value for the $4\ ^1P_1-1\ ^1S_0$ transition in P^{13+} are recommended as $21\,376\,454 \pm 350$ cm^{-1} (2650.34 ± 0.043 eV) in Ref. [23]. In Ref. [25] only transition energies were given, no transition strength was shown. In order to include the influence from the neighboring transitions, we perform a calculation on the energies and rates for the transitions among $1snl$ ($n \leqslant 6$) states in P^{13+} employing a combined relativistic configuration interaction and many-body perturbation theory method which has been implemented within the flexible atomic code (FAC) [26]. The detailed theoretical method was given in Ref. [27]. The key feature of the method is to divide the Hilbert space of the full Hamiltonian into a model space, *M*, and the orthogonal space, *N*. The Hamiltonian is taken to be the no-pair Dirac-Coulomb-Breit (DCB) Hamiltonian [28]. A non-Hermitian effective Hamiltonian is then constructed in the model space with perturbation expansion. The eigenvalues of this effective Hamiltonian give the level energies of the full Hamiltonian. With this method, the configuration interaction effects within the model space are exactly accounted for, while interaction between *M* and *N* are taken into account with the perturbation method. In the present work, the model space *M* contains all configurations of $1snl$ ($n \leqslant 6$) and the ground state $1s^2$. The *N* space contains all configurations that are single and double excitations of the *M* space, which are ones that enter the perturbation series up to the second order. The transition energy and rate of the $4\ ^1P_1-1\ ^1S_0$ line, as well as the other nearby lines, are listed in Table II. Considering the $4\ ^1P_1-1\ ^1S_0$ line may be blended with other lines, the final result 2650.34 ± 0.044 eV is obtained for the $4\ ^1P_1-1\ ^1S_0$ transition of the He-like *P*. The ± 0.044 eV uncertainty in the energy of the *P* reference line adds a systematic uncertainty to our measurement. By contrast, the uncertainties in the H-like S^{15+} line energies are small in comparison and can be neglected.

In order to get the calibration spectrum, *S* and *P* were injected into EBIT simultaneously. The effect of satellites from different charge states of *S* and *P* should be considered in the determination of the peak positions of the H-like *S* lines. It is found that two lines from the $(1s2p4d)_{1/2}-(1s^22s)_{1/2}$, $(1s2p4d)_{3/2}-(1s^22s)_{1/2}$ transitions and some lines from $1s2s5d-1s^22p$ transitions in the Li-like *P* ions will overlap with the Lyman-α lines. The calculated transition energies for two lines from $1s2p4d$ are 2620.12 eV and 2620.29 eV, respectively. The excitation cross section to such dielectronic states from the ground state of the Li-like ions is three orders smaller than that to the $1s4p\ ^1P_1$ state from the ground state in the He-like ions. Decay probability of such dielectronic state through autoionization is about one order in magnitude to that through radiative decay. If we assume the same amount of the He-like *P* ions and the Li-like *P* ions in the trap (usually more He-like ions than Li-like ions under rather high electron energy), these two dielectronic satellites will cause a shift of no more than 0.0001 eV in the wavelengths of the Lyman-α lines, and it corresponds to 0.001ch on the detector. The shift caused by $1s2s5d-1s^22p$ transitions is even smaller. Thus, compared with the uncertainty 0.022 channels, the effect of *S* and *P* injected simultaneously is negligible. And also from our calculation, the small peak appeares on the calibration spectrum at around 2643 eV is from the $1s2s5p-1s^22s$ transitions in the Li-like ions.

TABLE II. Transition energies (eV) and rates *A* (s^{-1}) for $1s4p\ ^1P_1-1s^2\ ^1S_0$ line and the nearby the $1s4l-1s^2\ ^1S_0$ lines. The superscripts of *A* indicate the kinds of multipole transitions, for example, A^{E1} represents the electric dipole transition rate in the He-like *P*.

Upper state	Energy	A^{E1}	A^{M2}	A^{E3}
$1s4p\ 4^1p_1$	2650.33	5.70×10^{12}		
$1s4p\ 4^3p_1$	2648.95	4.18×10^{10}		
$1s4p\ 4^3p_2$	2649.10		1.15×10^{7}	
$1s4f\ 4^3F_3$	2650.18			4.55×10^{5}
$1s4f\ 4^3F_2$	2650.18		3.27×10^{-1}	
$1s4f\ 4^1F_3$	2650.22			6.09×10^{5}
Upper state	Energy	A^{M1}	A^{E2}	A^{M3}
$1s4d\ 4^3D_1$	2650.06	2.00×10^{3}		
$1s4d\ 4^3D_2$	2650.06		6.70×10^{8}	
$1s4d\ 4^3D_3$	2650.12			1.25×10^{4}
$1s4d\ 4^1D_2$	2650.18		4.17×10^{9}	

For crystal x-ray spectroscopy, in order to obtain absolute wavelength determination to better than 100 ppm, a variety of effects in addition to refractive index corrections must be considered carefully [29]. Refractive index corrections occur at the level of 100–300 ppm and hence contribute to the major part of corrections. For flat crystals, usually thick flat crystals, the corresponding peak shift due to peak profile asymmetry must be included in high accuracy measurement. This may amount to more than one-half of the refractive index correction and will make a shift reducing the refractive index correction by up to 50% or more. These two effects are most important for absolute measurement using flat crystal x-ray spectroscopy. For curved crystals, curved crystal ge-

TABLE III. The error budget for the $1s^22p_{3/2}-1s^22s_{1/2}$ transition energy in $^{208}Pb^{79+}$.

Source of error	Error (eV)
Uncertainty in peak position for calibration line	0.022
Uncertainty in Pb line peak	0.022
Calibration wavelength	0.044
Dispersion relation due to locating calibration peaks	0.08
Isotope shifts and hyperfine splitting	0.018
Blending with other lines	≤0.01
Difference in refractive index correction	0.01
Total uncertainty	0.10

ometries are generally less affected by the peak profile asymmetry because the effective thickness leading to coherent diffraction is typically much less than the crystal thickness. Therefore, the magnitude of this correction is often reduced. Other qualitative effects introduced by curvature will also tend to dominate over those corrections common to the flat crystal case (for details, see Ref. [29]). However, in the current work, the wavelength is determined by calibration against other wavelengths, rather than using the Bragg relation, and so the absolute values of the systematic shifts arising from the dynamical theory are unimportant. According to the discussion in Ref. [10], it is important to consider the difference in refractive index correction across the energy range being studied. The appropriate rocking curve profiles for the Si(111) crystal are generated for two x-ray energies 2620 eV and 2650 eV. The angular shift of the highest points between the two sets of rocking curves is 2×10^{-6} rad for the π-polarization and 3×10^{-6} rad for the σ-polarization. The corresponding transition energy shifts are 0.005 eV and 0.01 eV, respectively. These uncertainties are shown in Table III.

The last part of total uncertainty for the $1s^22p_{3/2}-1s^22s_{1/2}$ transition energy in $^{208}Pb^{79+}$ is coming from the isotope shifts and hyperfine splitting of the ground state of the Li-like lead ions. We used natural lead for our experiment and therefore the injection element was a mixture of the four isotopes ^{204}Pb (1.48%), ^{206}Pb (23.6%), ^{207}Pb (22.6%), and ^{208}Pb (52.3%), where the percentages in the parentheses are the natural abundance. Considering the isotope shifts, the $1s^22p_{3/2}-1s^22s_{1/2}$ transition line for Pb^{79+} will separate into four lines with slightly different energies. By performing MCDF calculations using GRASP2K [30], allowing for single, double and triple excitations the isotope shifts relative to ^{208}Pb are predicted to be 0.1034 eV, 0.0516 eV, and 0.0258 eV for ^{204}Pb, ^{206}Pb, and ^{207}Pb, respectively.

A further complication of the system is due to the nuclear spin, $I=1/2$, of ^{207}Pb which splits the line into three different hyperfine components. Using the standard formula for hyperfine splitting due to nuclear magnetic dipole interaction,

$$\Delta E = A/2[F(F+1) - J(J+1) - I(I+1)],$$

where A is the hyperfine constant. The hyperfine splitting of the ground state $2s_{1/2}$ was calculated and was predicted to

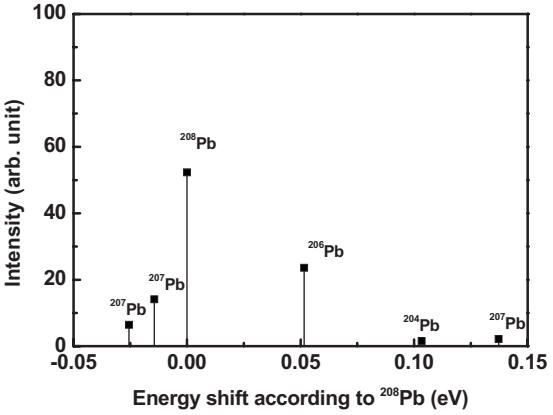

FIG. 4. Energy shifts of the $1s^22p_{3/2}-1s^22s_{1/2}$ transitions in the Li-like nature lead ions according to the hyperfine splitting and isotope shifts.

0.1887(9) eV [31]. From the formula above, the shift of the $2s_{1/2}$ $F=0$ hyperfine level is shifted by $\Delta E_{2sF=0}=-3A_{2s}/4$ and the $F=1$ level is shifted by $\Delta E_{2sF=1}=A_{2s}/4$ and $A_{2s}=0.1887(9)$ eV. To predict the hyperfine splitting of the $2p$ state, MCDF calculations using GRASP2K is performed and the hyperfine constant A_{2p} is found to be 0.0056 eV. Using this value and the isotope shift of ^{207}Pb, the energy shifts of the hyperfine lines relative to ^{208}Pb could be predicted to −0.0144 eV for the $F=2-F=1$ transition, −0.0256 eV for the 1–1 transition, and 0.1373 eV for the 1–0 transition.

Including the isotope shifts and hyperfine splitting, finally we have six lines spread out in a range of 0.1517 eV. By using the abundance of the different isotopes and relative intensities of the hyperfine lines, we could predict how intense the different lines should be. Out of the whole intensity of the spectrum of these lines, 52.3% should be from ^{208}Pb, 23.6% from ^{206}Pb (shifted 0.0516 eV), 1.5% from ^{204}Pb (shifted 0.1034 eV), and 22.6% should come from the three components of ^{207}Pb. If we assume that the relative population of the two upper hyperfine levels of ^{207}Pb are equal to the degeneracy of the states and use the relative intensities of different hyperfine transitions from an upper level to a set of lower which is given by 6J symbols, we find that the intensities ratio of these lines should be $I(1-0):I(1-1):I(2-1)=1:3:6.67$. Including the abundance of ^{207}Pb, the relative intensity of the 2–1 line should be 14.1% (shifted −0.0144 eV), the 1–1 line 6.4% (shifted −0.0256 eV), and the 1–0 line 2.1% (shifted 0.1373 eV).

Figure 4 shows the energy shifts of the $1s^22p_{3/2}-1s^22s_{1/2}$ transitions in the Li-like nature lead ions. The separations are smaller than the energy resolution of the flat crystal spectrometer (~0.5 eV) in the Pb measurement. Therefore, the separations could not be resolved in our measurement, only one peak was observed. From the fitting of the Li-like P line, the Lorentzian line profile is found and the full width at half-maximum (FWHM) is 0.5 eV. Then we spread these lines by the Lorentzian formula with 0.5 eV FWHM, and then fit the sum of six spectra by also the Lorentzian, it is found that the final peak is 0.018 eV shift to the higher energy side of the ^{208}Pb peak. Therefore, we introduce additional energy uncertainty 0.018 eV for the determination of

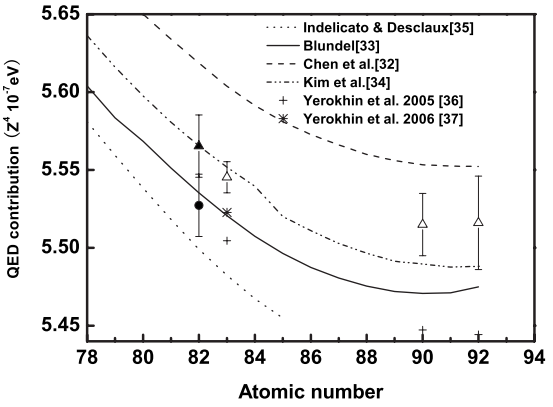

FIG. 5. Comparison of the measured and calculated QED contribution to the $1s^22p_{3/2}-1s^22s_{1/2}$ transition in highly charged Li-like ions. Solid circle, present measurement subtracting non-QED parts in text; solid triangle, present measurement subtracting non-QED parts by Chen *et al.* as in other measurements; open triangle, experimental data from Ref. [3]. Lines, crosses, and stars are theoretical values, from [32–37].

the energy of the $1s^22p_{3/2}-1s^22s_{1/2}$ transition in $^{208}Pb^{79+}$.

The error budget for this experiment is given in Table III. Besides the uncertainties of the peak positions of the calibration lines (± 0.022 eV), the uncertainty of the position of the Pb line (± 0.022 eV), the systematic uncertainty associated with the uncertainty in the wavelength of the $4p-1s$ transition in He-like *P* calibration line (± 0.044 eV), the uncertainty (± 0.08 eV) introduced by the determination of dispersion relation from the calibration lines must be included and it is the dominant contribution to the total uncertainty. Table III also shows the peak shift due to peak blending resulting from the isotope shifts and hyperfine splitting in the Li-like Pb ions and the transition energy shift due to the difference in refractive index correction in the interested energy range. Blending with other lines for the measurement of the $1s^22p_{3/2}-1s^22s_{1/2}$ transition in $^{208}Pb^{79+}$ is estimated to be no more than 0.01 eV.

V. COMPARISON WITH THEORY

In Fig. 5, the measured QED value is compared with available calculations: *Ab initio* calculations of the screened QED terms performed by Chen *et al.* [32] and Blundell [33]. Also shown are the QED values calculated by Kim *et al.* [34], by Indelicato and Desclaux [35] using screened hydrogenic values. Figure 5 also shows experimental results for the measurement of the $1s^22p_{3/2}-1s^22s_{1/2}$ transition in other Li-like heavy ions [3], and the new calculation results by Yerokhin *et al.* [36,37]. It can be seen that, from the trend of available high *Z* experimental results, our measurement will agree with the calculated QED contributions by Yerokhin *et al.* at $Z=82$, although there has been no calculation carried out that includes higher-order QED effects. One interesting thing is that the experimental result for Pb also agrees with the calculation results by Blundell well.

VI. CONCLUSION

The $1s^22p_{3/2}-1s^22s_{1/2}$ x-ray transition in the Li-like Pb^{79+} has been observed with a flat crystal x-ray spectrometer that consists of a Si(111) crystal and a back-illuminated CCD at the Tokyo EBIT. Pb was injected into the EBIT using an effusion cell. The measurement was made by calibrating the Pb lines using the Lyman-α lines of the H-like *S* and the $4p-1s$ transition in the He-like *P*. Sulfur was injected through a gas injector as SF_6 while phosphorus was injected from the gas injection port using the vapor of diethyl phosphite (liquid). The energy of the $1s^22p_{3/2}-1s^22s_{1/2}$ transition in $^{208}Pb^{79+}$ has been determined to be 2642.26 ± 0.10 eV. It can be seen from the error budget that the rather large uncertainty in the line's peak position (± 0.22 channels) introduces large error in the dispersion relation determination, and is the dominant contribution in the determination of energy of the $1s^22p_{3/2}-1s^22s_{1/2}$ transition in the Li-like Pb^{79+}. It means that the experimental system (including the spectrometer and the EBIT source) should be stable enough to get results with much higher accuracy.

The contribution of QED (-24.99 ± 0.10 eV) is extracted. The measured QED value is compared with available calculations: *Ab initio* calculations of the screened QED terms performed by Chen *et al.* and Blundell; calculations by Kim *et al.*, by Indelicato and Desclaux using screened hydrogenic values; the calculations by Yerokhin *et al.* In conjunction with other experimental results of Bi^{80+}, Th^{87+}, and U^{89+}, the measurements clearly distinguish between calculations.

As seen in the experimental uncertainty part, contribution due to isotope shifts and hyperfine splitting will make the analysis much more complicated. Therefore, the isotope-pure element will be a better candidate for such measurement, and the element with even mass number and even nuclear number will be preferred.

ACKNOWLEDGMENTS

We acknowledge Professor Roger Hutton, Professor Yaming Zou, and Ke Yao for helpful discussion. This work was performed under the auspices of the Japan-China Core University Program in Plasma and Fusion Research, The CREST program, and the 21st COE program. One of the authors (X.Z.) is grateful to the group of Tokyo EBIT for their hospitality, and was partly supported by the National Natural Science Foundation of China under Grants No. 10434050 and No. 10774026, by the program for New Century Excellent Talents in University (NCET), and by the Shanghai Leading Academic Discipline Project under Contract No. B107.

[1] P. Beiersdorfer, D. Knapp, R. E. Marrs, S. R. Elliott, and M. H. Chen, Phys. Rev. Lett. **71**, 3939 (1993).
[2] P. Beiersdorfer, A. Osterheld, S. R. Elliott, M. H. Chen, D. Knapp, and K. Reed, Phys. Rev. A **52**, 2693 (1995).
[3] P. Beiersdorfer, A. L. Osterheld, J. H. Scofield, J. R. Crespo López-Urrutia, and K. Widmann, Phys. Rev. Lett. **80**, 3022 (1998).
[4] P. Beiersdorfer, H. Chen, D. B. Thorn, and E. Träbert, Phys. Rev. Lett. **95**, 233003 (2005).
[5] C. Brandau, C. Kozhuharov, A. Müller, W. Shi, S. Schippers, T. Bartsch, S. Böhm, C. Böhme, A. Hoffknecht, H. Knopp, N. Grün, W. Sheid, T. Steih, F. Bosch, B. Franzke, P. H. Mokler, F. Nolden, M. Steck, T. Stöhlker, and Z. Stachura, Phys. Rev. Lett. **91**, 073202 (2003).
[6] P. H. Mokler, Radiat. Phys. Chem. **75**, 1730 (2006).
[7] Nobuyuki Nakamura, Junji Asada, Frederick J. Currell, Tsunemitsu Fukami, Takato Hirayama, Kenji Motohashi, Tetsuo Nagata, Eimitsu Nojikawa, Shunsuke Ohtani, Kiyohiko Okazaki, Makoto Sakurai, Hiroshi Shiraishi, Seiji Tsurubuchi, and Hirofumi Watanabe, Phys. Scr., T **T73**, 362 (1997).
[8] Chikashi Yamada, Kazuo Nagata, Nobuyuki Nakamura, Shunsuke Ohtani, Satoshi Takahashi, Hirotsugu Tobiyama, Masahide Tona, Hirofumi Watanabe, Nobuo Yoshiyasu, Makoto Sakurai, Anthony P. Kavanagh, and Fred J. Currell, Rev. Sci. Instrum. **77**, 066110 (2006).
[9] Nobuyuki Nakamura, Rev. Sci. Instrum. **71**, 4065 (2000).
[10] C. T. Chantler, D. Paterson, L. T. Hudson, F. G. Serpa, J. D. Gillaspy, and E. Takacs, Phys. Rev. A **62**, 042501 (2000).
[11] M. R. Tarbutt and J. D. Silver, J. Phys. B **35**, 1467 (2002).
[12] V. A. Yerokhin, A. N. Artemyev, and V. M. Shabaev, Phys. Rev. A **75**, 062501 (2007).
[13] A. N. Artemyev, V. M. Shabaev, and V. A. Yerokhin, Phys. Rev. A **52**, 1884 (1995).
[14] A. N. Artemyev, V. M. Shabaev, and V. A. Yerokhin, J. Phys. B **28**, 5201 (1995).
[15] G. Plunien and G. Soff, Phys. Rev. A **51**, 1119 (1995).
[16] A. V. Nefiodov, L. N. Labzowsky, G. Plunien, and G. Soff, Phys. Lett. A **222**, 227 (1996).
[17] F. A. Parpia, C. F. Fischer, and I. P. Grant, Comput. Phys. Commun. **94**, 249 (1996).
[18] I. P. Grant and H. M. Quiney, Adv. At. Mol. Phys. **23**, 37 (1988).
[19] P. Jönsson, F. A. Parpia, and C. F. Fischer, Comput. Phys. Commun. **96**, 301 (1996).
[20] J. P. Desclaux, C. M. Moser, and G. Verhaegen, J. Phys. B **4**, 296 (1971).
[21] C. F. Fischer, Comput. Phys. Commun. **64**, 369 (1991).
[22] C. F. Fischer and P. Jönsson, Comput. Phys. Commun. **84**, 37 (1994).
[23] L. W. Fullerton and G. A. Rinker, Phys. Rev. A **13**, 1283 (1976).
[24] W. C. Martin, Romuald Zalubas, and Ariene Musgrove, J. Phys. Chem. Ref. Data **19**, 821 (1990).
[25] W. C. Martin, Romuald Zalubas, and Ariene Musgrove, J. Phys. Chem. Ref. Data **14**, 751 (1985).
[26] M. F. Gu, Astrophys. J. **582**, 1241 (2003).
[27] M. F. Gu, T. Holczer, E. Behar, and S. M. Kahn, Astrophys. J. **641**, 1227 (2006).
[28] J. Sucher, Phys. Rev. A **22**, 348 (1980).
[29] C. T. Chantler and R. D. Deslattes, Rev. Sci. Instrum. **66**, 5123 (1995).
[30] P. Jönsson, X. He, C. Froese Fischer, and I. P. Grant, Comput. Phys. Commun. **177**, 597 (2007).
[31] V. M. Shabaev, M. B. Shabaeva, I. I. Tupitsyn, V. A. Yerokhin, A. N. Artemyev, T. Kühl, M. Tomaselli, and O. M. Zherebtsov, Phys. Rev. A **57**, 149 (1998).
[32] M. H. Chen, K. T. Cheng, W. R. Johnson, and J. Sapirstein, Phys. Rev. A **52**, 266 (1995).
[33] S. A. Blundell, Phys. Rev. A **47**, 1790 (1993).
[34] Y.-K. Kim, D. H. Baik, P. Indelicato, and J. P. Desclaux, Phys. Rev. A **44**, 148 (1991).
[35] P. Indelicato and J. P. Desclaux, Phys. Rev. A **42**, 5139 (1990).
[36] V. A. Yerokhin, A. N. Artemyev, V. M. Shabaev, G. Plunien, and G. Soff, Opt. Spectrosc. **99**, 12 (2005).
[37] V. A. Yerokhin, P. Indelicato, and V. M. Shabaev, Phys. Rev. Lett. **97**, 253004 (2006).